

# Negative Masses and Spatial Curvature: Alleviating Neutrino Mass Tensions in $\Lambda$ CDM and Extended Cosmologies

Hayyim Pulido-Hernández<sup>1,2,\*</sup> and Jorge L. Cervantes-Cota<sup>1,†</sup>

<sup>1</sup>*Departamento de Física, Instituto Nacional de Investigaciones Nucleares, Apartado Postal 18-1027, Col. Escandón, Ciudad de México, 11801, México.*

<sup>2</sup>*Instituto de Física, Universidad Nacional Autónoma de México, Apartado Postal 20-364, Ciudad Universitaria, Ciudad de México, 04510, México.*

(Dated: March 16, 2026)

We investigate the impact of spatial curvature,  $\Omega_k$ , and dynamical dark energy on the cosmological constraints of the neutrino mass sum,  $\sum m_\nu$ . Using a joint analysis of the latest CMB (Planck and ACT DR6), BAO (DESI DR2) and SNe Ia (DESY5 and DES-Dovekie) datasets, we perform an exploration of the neutrino mass parameter space. To mitigate prior-driven biases near the physical boundary, we implement a symmetric extension wrapper that allows for effective negative masses. We find that the inclusion of spatial curvature significantly modifies the posterior distributions, exhibiting a smooth transition across the  $\sum m_\nu = 0$  threshold. In the  $\Lambda$ CDM +  $\Omega_k$  +  $\sum m_{\nu,eff}$  framework, we obtain  $\sum m_{\nu,eff} = -0.011^{+0.052}_{-0.050}$ , reducing the tension with the terrestrial lower limit of 0.06 eV from  $2.59\sigma$  for the  $\Lambda$ CDM +  $\sum m_{\nu,eff}$  model to  $1.17\sigma$ . For the most flexible scenario  $\omega_0\omega_a$ CDM +  $\Omega_k$  +  $\sum m_{\nu,eff}$ , we find  $\sum m_{\nu,eff} = -0.07 \pm 0.11$  with a tension of  $1.13\sigma$ , illustrating how the increased parameter freedom notably degrades the precision of the mass estimate compared to simpler extensions. Our results demonstrate that current cosmological bounds on  $\sum m_\nu$  are heavily influenced by boundary effects and geometric degeneracies.

Keywords: large scale structure formation. neutrino mass. cosmological curvature.

## CONTENTS

I. Introduction	1
II. Neutrino mass effects, cosmic probes, and models	2
III. Numerical Implementation and datasets	4
A. Effective neutrino mass	4
B. Datasets for the analysis	5
IV. Results	6
A. $\Lambda$ CDM model	6
B. $\omega_0\omega_a$ CDM Model	7
C. Effective neutrino mass results	8
D. Goodness of fit	9
V. Conclusions	10
VI. Acknowledgments	12
References	13
A. Dovekie results	15
B. Best-fit results for all cosmological parameters	16

## I. INTRODUCTION

The standard model of cosmology assumes its visible components are baryons and photons, from which we have an overwhelming direct evidence, and it also adds dark matter and dark energy, from which we perceive only its gravitational effects. The last piece is neutrinos; they are known to possess mass. Recent results from the ground-based neutrino oscillation experiments pose, on the one hand, a lower bound  $\sum m_\nu > 0.059$  eV for normal mass ordering and  $\sum m_\nu > 0.1$  eV for inverted mass ordering [1]. On the other hand, an upper bound comes from the KATRIN experiment, that when combined with oscillation results, leads to the limit  $\sum m_\nu < 1.35$  eV at 90% cl. [2–4].

The determination of neutrino mass through cosmological observables has been an active and fruitful area of research for decades. Since the first estimate in 1966 using astronomical measurements [5], followed by the first measurement using modern methodology in 1999 [6], both the precision and volume of available data have increased significantly. Today, the availability of large-scale datasets and enhanced computational power allow cosmologists to test a wide range of data and model combinations, aiming to resolve the inconsistencies currently present in the standard cosmological model. Neutrino masses enter naturally in discussion since they provoke effects in the Hubble expansion rate, CMB power spectra, and clustering properties of large scale structure. The measurement of neutrino masses has thus become a central objective of major astronomical collaborations.

\* alambhayim@estudiantes.fisica.unam.mx

† jorge.cervantes@inin.gob.mx

However, as cosmological data have reached unprecedented precision, a new challenge has emerged: the neutrino mass sum inferred from cosmological observables is in significant tension with the lower bounds established by terrestrial experiments. In fact, posterior probabilities resulting from the cosmological inference in the  $\Lambda$ CDM model seem to prefer negative values. This is not a recent artifact, as early results from the Planck collaboration already hinted at this trend [7], which has been only amplified with subsequent data releases [8–11]. Most recently, the DESI collaboration has reported the most stringent constraints to date, which simultaneously represent the highest level of tension with local measurements [12, 13].

On the other hand, the DESI results also indicate a preference for alternative dark energy models, specifically the Chevallier-Polarski-Linder (CPL, also named  $\omega_0\omega_a$ CDM) parameterization [14, 15]. This parameterization, however, changes the inferred value of the matter energy density ( $\Omega_m$ ), that in turn affects the neutrino mass. The synergy between DESI’s precise  $\Omega_m$  measurements and additional datasets, such as CMB, CMB Lensing, and Supernovae type Ia (SN Ia), allows for the breaking of key parameter degeneracies, most notably for the present work, those involving spatial curvature,  $\Omega_k$ . While the flat-Universe baseline model is standard, treating  $\Omega_k$  as a free parameter significantly impacts the total matter density and, consequently, the inferred  $\sum m_\nu$ . Recent investigations have demonstrated that exploring curved cosmologies can effectively mitigate the tension with terrestrial constraints [16].

Alongside by these developments, this work provides a comprehensive extension to the current literature by analyzing the  $\omega_0\omega_a$ CDM framework in conjunction with the spatial curvature and also exploring the negative neutrino mass scenario. Although a negative mass is physically nonsensical within the current paradigm, it serves as a valuable phenomenological approach to identify the di-

rections in which current datasets pull the model. To this end, we adopt and numerically implement the methodology proposed in Ref. [17] for an effective neutrino mass sum.

The structure of this work is organized as follow: Section II discusses the cosmological role of neutrinos and their interplay with our chosen datasets. Section III details the numerical implementation of the effective neutrino mass and the sampling configuration. Our main findings are presented and discussed in Section IV. In Section V we summarize our findings and conclude. Finally, Appendix A reports relevant results utilizing the most recent supernova recalibration.

## II. NEUTRINO MASS EFFECTS, COSMIC PROBES, AND MODELS

Although terrestrial experiments can impose upper [2–4] or lower [1, 18, 19] bounds on the sum of neutrino masses, the most restrictive constraints arise from cosmological measurements [13, 20]. Through the evolution of the Universe, neutrinos are the only particles that transition from relativistic behavior in the early Universe to behaving as cold dark matter in the late Universe. This transition affects the dynamics in various ways, modifying the cosmological observables. The bounds imposed by terrestrial measurements imply that neutrinos begin to behave as dark matter well after the epoch of recombination. Consequently, neutrinos have two primary implications in Large Scale Structure [21]: they modify the geometry of the Universe and suppress the growth of large-scale structure.

When influencing the cosmic geometry, neutrinos modify the cosmological distances. For the background evolution, a fundamental expression is the Friedmann equation, which takes the form:

$$\frac{H^2(z)}{H_0^2} = \Omega_r(1+z)^4 + \Omega_m(1+z)^3 + \Omega_k(1+z)^2 + \Omega_{DE} \frac{\rho_{DE}(z)}{\rho_{DE,0}} + \Omega_\nu \frac{\rho_\nu(z)}{\rho_{\nu,0}} \quad (1)$$

where the  $\Omega_i$  are the known density parameters evaluated at present times, and  $\Omega_\nu$  is the neutrino density given by

$$\Omega_\nu = \frac{\sum m_\nu}{93.14h^2 \text{ eV}}, \quad (2)$$

where  $h$  is given by  $H_0 = 100 h \text{ km s}^{-1}\text{Mpc}^{-1}$ . Furthermore, a key observable quantity is the *transverse comoving distance*, defined as [22]:

$$D_M(z) = \begin{cases} \frac{1}{H_0\sqrt{\Omega_k}} \sinh \left[ \sqrt{\Omega_k} \frac{\chi(z)}{1/H_0} \right] & \text{for } \Omega_k > 0 \\ \chi(z) & \text{for } \Omega_k = 0 \\ \frac{1}{H_0\sqrt{|\Omega_k|}} \sin \left[ \sqrt{|\Omega_k|} \frac{\chi(z)}{1/H_0} \right] & \text{for } \Omega_k < 0 \end{cases} \quad (3)$$

where the line-of-sight comoving distance is

$$\chi(z) = \int_0^z \frac{dz'}{H(z')}. \quad (4)$$

All other observable cosmological distances are derived from (4) and the Hubble function,  $H(z)$ . As we can see from equations (1-3), the sum of neutrino masses affects the cosmic expansion history. This primarily affects low-redshift observations, and although the effect is tiny, a key point is the precise determination of  $\Omega_m$  in equation (1), since it conditions the influence of the neutrino mass that, in late times, behaves as dark matter.

The primary probes for these distance measurements are Baryon Acoustic Oscillations (BAO) and Type Ia Supernovae (SNe Ia), while Cosmic Microwave Background (CMB) data provide a precise determination of the matter density through the full temperature and polarization power spectra and through the angular scale of the sound horizon,  $\theta_*$ . The tight constraints on  $\theta_*$  provided by the CMB induce a geometric degeneracy between  $\Omega_m$  and  $\sum m_\nu$ . Following the arguments in Ref. [21], maintaining the observed angular scale requires  $\Omega_m$  to adjust in response to changes in the sum of the neutrino masses.

On the other hand, there is a suppression of the large-scale structure caused by massive neutrinos. Although at late times neutrinos behave as dark matter, they retain thermal velocities high enough to inhibit the growth of structure on small scales. While neutrinos are relativistic, their free-streaming length,  $x_{fs}$ , is of the order of the Hubble radius. As the Universe evolves, this length decreases, and the free-streaming scale defined as  $k_{fs} = 1/x_{fs}$  takes the form [23]:

$$k_{fs}(z) \approx 0.0908 \frac{H(z)}{(1+z)^2} \left( \frac{m_\nu}{0.1eV} \right) hMpc^{-1}. \quad (5)$$

The streaming effect applies to every neutrino mass that, for simplicity, we assume here is degenerate. Any matter overdensity with a radius smaller than the free-streaming length will be attenuated. This suppression of large-scale structure primarily affects the matter power spectrum, although it also has detectable consequences in the CMB [21, 24]. To characterize the cutoff in the matter spectrum induced by free-streaming, a Full-Shape analysis can be employed. Given the precision of the datasets, it has not yet been detected; therefore, we will not employ a Full-Shape analysis here.

On the other hand, an important perturbative implication of neutrino mass originates when CMB photons travel from the surface of last scattering toward us, and their trajectories are deflected by the gravitational potential of the large-scale structures along their path. This phenomenon, known as CMB lensing, acts as a probe of the matter distribution to which neutrinos also contribute, allowing for the extraction of indirect but robust information regarding their masses. That is why, in this analysis, CMB lensing is also included.

Consequently, it is imperative to combine multiple observables such as BAO, SNe Ia, CMB, and CMB Lensing to break the parameter degeneracies inherent in each individual survey. However, a significant challenge arises when utilizing the latest datasets, as their respective estimates for  $\Omega_m$  show mutual inconsistency in the  $\Lambda$ CDM model. Specifically, DESI BAO measurements report low values ( $\Omega_m = 0.2975 \pm 0.0086$  [12]), while Planck CMB data favor intermediate results ( $\Omega_m = 0.3166 \pm 0.0084$  [25]), and supernova surveys suggest even higher densities ( $\Omega_m > 0.35$ ) [26–28]. The discrepancy among these datasets creates a tension in the determination of the expansion history.

Consequently, to reconcile the matter density value, the statistical fit is driven towards an effective negative neutrino mass as a compensatory mechanism [21].

Another relevant extension to this analysis is the study of spatial curvature. While a spatially flat Universe ( $\Omega_k = 0$ ) is conventionally assumed, CMB measurements exhibit a significant geometrical degeneracy between curvature and the matter density  $\Omega_m$ . Breaking this degeneracy requires the inclusion of other probes, such as supernovae or BAO, which provide robust constraints on  $\Omega_m$ . This interplay directly affects neutrino mass estimates, as neutrinos contribute to the total matter density at late times. Ref. [16] provides a thorough exploration of these physical effects within the  $\Lambda$ CDM model, demonstrating that allowing for non-zero spatial curvature can alleviate the tension between cosmological bounds and terrestrial neutrino mass measurements. In this work, we consider curvature in our analysis.

On the theoretical side, the matter and neutrino density parameters, as seen in Eq. (1), depend on the DE model. To explore extensions beyond the  $\Lambda$ CDM model, one may adopt the CPL parametrization, also referred to as  $\omega_0\omega_a$ CDM. In this framework, the evolution of the dark energy density in (1) is governed by a time-dependent equation-of-state parameter, defined as:

$$\omega(z) = \omega_0 + \omega_a \frac{z}{1+z} \quad (6)$$

where  $\omega_0$  and  $\omega_a$  are the parameters to be determined. One normally expects that parameter inferences should yield results in which  $\omega_0 = -1$  and  $\omega_a = 0$  are within error bars that include the  $\Lambda$ CDM model. But recent results from DESI have shown a tension of 1.7-4.2 $\sigma$  relative to  $\Lambda$ CDM, depending on the specific combination of datasets employed [12]; see, however, Ref. [29] for a reanalysis finding a lower tension. This discrepancy motivates the exploration of scenarios involving dynamical dark energy.

To illustrate the current observational landscape, Table I provides a detailed compendium of reported bounds on  $\sum m_\nu$ . The results are presented as a function of the various cosmological models and data combinations employed in each study, allowing for the identification of how these constraints vary across different assumptions and observational samples. This comparison facilitates an analysis of the impact that both model choice and data selection have on the precision of the resulting limits.

Dataset	$\sum m_\nu$ [eV] (95%)
<b><math>\Lambda</math>CDM Model</b>	
DESIDR2+CMB	< 0.0642 [13]
DESIDR2+CMB+DESY5	< 0.0744 [13]
DESIDR2+CMB+Union3	< 0.0674 [13]
DESIDR2+CMB+Pantheon+	< 0.0704 [13]
DESIDR1(FS+BAO)+BBN+ $n_s$	< 0.300 [13]
DESIDR1(FS+BAO)+BBN+(\(\theta_s, n_s\)) <sub>CMB</sub>	< 0.193 [13]
DESIDR2+CMB+DESY5+DESY1(WL)	< 0.085 [30]
<b><math>\omega</math>CDM Model</b>	
DESIDR2 + CMB	< 0.0851 [13]
DESIDR2 + CMB + DESY5	< 0.0586 [13]
DESIDR2 + CMB + Union3	< 0.0649 [13]
DESIDR2 + CMB + Pantheon+	< 0.0653 [13]
DESIDR2+CMB+DESY5+DESY1(WL)	< 0.065 [30]
<b><math>\omega_0\omega_a</math>CDM Model</b>	
DESIDR2 + CMB	< 0.163 [13]
DESIDR2 + CMB + DESY5	< 0.129 [13]
DESIDR2 + CMB + Union3	< 0.139 [13]
DESIDR2 + CMB + Pantheon+	< 0.117 [13]
DESIDR2+CMB+DESY5+DESY1(WL)	0.098 <sup>+0.016</sup> <sub>-0.037</sub> [30]
<b>Matter Conversion Model</b>	
DESIDR2 + CMB(No Lensing)	0.106 <sup>+0.050</sup> <sub>-0.069</sub> [31]
<b>EDE Model</b>	
DESIDR1+CMB	< 0.097 [32]
<b>Sound Horizon Agnostics</b>	
DESIDR2+Lensing+Pantheon++DESY3(WL)	0.55 <sup>+0.23</sup> <sub>-0.37</sub> [33]
IDL+unSNeIa+KiDS+BBN+ $A_s+n_s$	1.08 <sup>+0.65</sup> <sub>-0.60</sub> [34]
IDL+unSNeIa+KiDS+BBN++ $A_s+n_s$ +Lensing(No SPT-3G)	1.01 <sup>+0.52</sup> <sub>-0.46</sub> [34]
<b><math>\tau</math> modification</b>	
DESIDR1+CMB(NoLow $\ell$ , NoLensing)	0.01 $\pm$ 0.06 [35]

TABLE I: Compendium of recent estimates for  $\sum m_\nu$  across various cosmological models and datasets. Although the DESI collaboration [13] provides the most extensive set of measurements, their results for the negative mass regime are omitted in this table for brevity. Notably, Ref. [30] establishes a Gaussian constraint within the positive mass range using weak lensing data. Finally, recent studies [31, 35] illustrate the diverse strategies for addressing the neutrino mass tension; there is a growing trend toward modifying early-Universe physics.

### III. NUMERICAL IMPLEMENTATION AND DATASETS

Our parameter estimation is performed via Markov Chain Monte Carlo (MCMC) sampling, specifically employing the Metropolis-Hastings algorithm within the cosmological inference code **Cobaya** [36, 37]. Our analysis utilizes the Boltzmann solver **CAMB** [38] for positive neutrino mass priors and CLASS [39, 40] for the runs that include the negative mass regime, as well as Cobaya’s public likelihoods. We run four independent chains in parallel for each case. Furthermore, point estimates for the best-fit parameters are obtained using the **iminuit** minimizer integrated within Cobaya. The convergence of the MCMC is determined by the Gelman-Rubin statistics [41], requiring  $R - 1 < 0.01$ . Post-processing is done using the **GetDist** Python package [42].

#### A. Effective neutrino mass

As mentioned, Table I illustrates recent findings reported within the standard framework in which neutrino masses are always positive. While a negative mass for a particle lacks any physical meaning, as we discussed in Section II, various results exhibit a tension with the limits established by terrestrial experiments and even their posterior probabilities lies in the negative values, when one allows for it [13, 35, 37, 43, 44]. To find out whether this is really the case, that data prefer negative masses, a methodology has recently been put forward [17]. In that work, two approaches were presented. The first, named the *exact method*, consists of modifying the background and perturbative equations as follows

$$\begin{aligned} \epsilon_{eff} &= \text{sgn}(m_\nu) \sqrt{x^2 + a^2 m_\nu^2 / T_\nu^2} \\ \dot{\Psi}_0 &= -\frac{qk}{\epsilon_{eff}} \Psi_1 - \phi \frac{d \ln \bar{f}}{d \ln q}, \quad \dot{\Psi}_1 = \frac{qk}{3\epsilon_{eff}} (\Psi_0 - 2\Psi_2) - \frac{\epsilon_{eff} k}{3q} \psi \frac{d \ln \bar{f}}{d \ln q} \\ \dot{\Psi}_\ell &= \frac{qk}{(2\ell + 1)\epsilon_{eff}} [\ell \Psi_{\ell-1} - (\ell + 1)\Psi_{\ell+1}], \quad (\ell \geq 2) \end{aligned} \quad (7)$$

where  $\epsilon_{eff}$  is the effective neutrino energy parameter and  $\Psi_\ell$  are the distribution function perturbation multipole moments in the Newtonian gauge [45].

The second approach is the *extrapolation method*, which requires modifying a physical observable  $X$  that depends on a set of parameters  $\theta$ .

$$X_\theta^{\sum m_{\nu,eff}} \equiv X_\theta^{\sum m_{\nu=0}} + \text{sgn} \left( \sum m_{\nu,eff} \right) \left[ X_\theta^{|\sum m_{\nu,eff}|} - X_\theta^{\sum m_{\nu=0}} \right]. \quad (8)$$

The first method requires a modification of the cosmo code in CAMB or CLASS, whereas the second method demands to modify the interface between CLASS and Cobaya. Since both methods yield the same results, we thus chose the extrapolation method in this work.

The implementation requires determining the value of the `m_ncdm` variable at each step of the Cobaya sampler; this variable defines the neutrino mass within CLASS. Two scenarios then arise:

- A. If `m_ncdm`  $\geq 0$ : Cobaya and CLASS execute normally.
- B. If `m_ncdm`  $< 0$ : CLASS is executed twice to obtain  $X_\theta^{|\sum m_{\nu,eff}|}$  and  $X_\theta^{\sum m_{\nu=0}}$  for each observable required by Cobaya, followed by the application of Eq. (8).

To validate the implementation, Figure 1 displays the results obtained to verify the correct functioning of the code. In the upper panel, we confirm that the direct application of extrapolation method within CLASS is the same as the computation performed via Cobaya. Furthermore, the lower panel shows an agreement of our results and those presented in [13].

## B. Datasets for the analysis

Our objective is to obtain constraints on  $\sum m_\nu$ , considering positive and negative priors on it, and to understand the role played by curvature and the dark energy parameters  $w_0$  and  $w_a$  of the CPL parameterization. For this purpose, we have employ the subsequent datasets, with our baseline configuration including:

- **BAO**: We use BAO data from DESI DR2 [12] using all of the tracers.
- **CMB**: We use the Planck 2018 [25] PR3 low- $\ell$  for TT and EE modes and PR4 high- $\ell$  CamSpec [46–49] TTTEEE likelihoods. Additionally, we use the combination of Planck and ACT DR6 CMB lensing [50–52].
- **SNe Ia**: We use the DESY5 [26] likelihood for supernovae measurements.

This specific data, when analyzed individually, imply a tension in the inferred  $\Lambda$ CDM cosmological parameters, e.g. in  $\Omega_m$ . While this would, in principle, be a reason to be cautious in its use, we have chosen this data setup for two primary reasons: first, to examine the behavior of parameter estimates under  $\Lambda$ CDM extensions and alternative models; and second, to ensure the inclusion of the most recent data releases, omitting the Planck Lollipop and HiLLiPoP likelihoods as CamSpec likelihoods yields equivalent results [53] while reducing the overall computational time.

In addition to this setup, recently, a recalibration of the DESY5 data was released, designated as DESY5-Dovekie [54]; we present the results corresponding to this updated dataset in Appendix A.

Our runs make use of the set of seven cosmological parameters  $(100\theta_*, \ln(10^{10} A_s), n_s, \tau, \omega_{cdm}, \omega_b, \Omega_k)$ , where  $\theta_*$  is the he acoustic angular scale,  $\ln(10^{10} A_s)$  and  $n_s$  are the amplitude and spectral index of the primordial scalar perturbations, respectively,  $\tau$  is the reionization optical depth,  $\omega_{cdm}$  and  $\omega_b$  are the physical abundance of cold dark matter and baryons, respectively, and  $\Omega_k$  is the spatial curvature parameter.

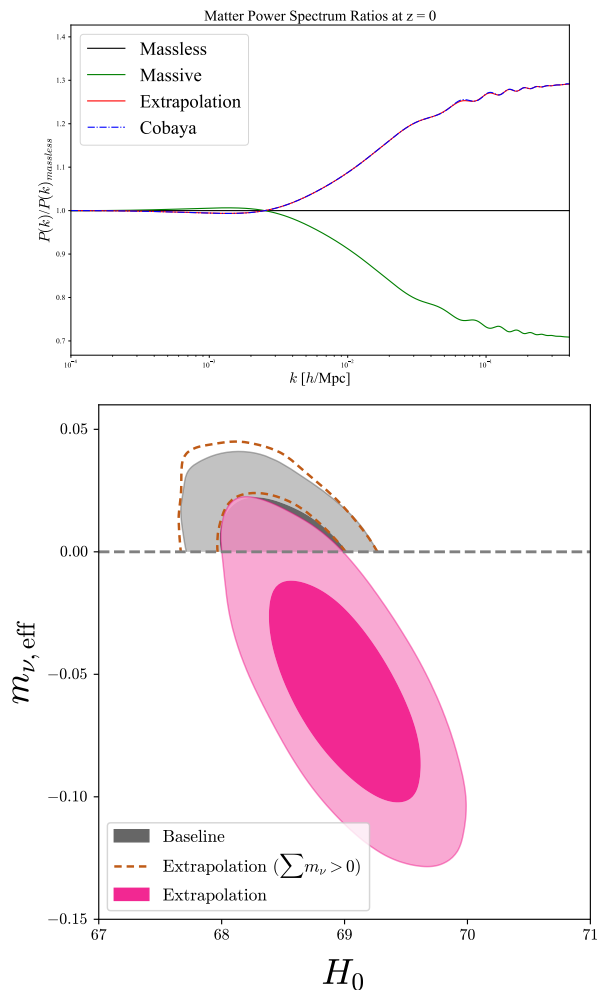


FIG. 1: Validation of the code implementation for the extrapolation method. **(Upper)** Comparison of ratios between negative mass scenarios and the massless case; the red line represents the direct application of Eq. (8) within CLASS, while the blue line corresponds to the computation performed via the Cobaya `get_model()` function. **(Lower)** Posterior contours comparing the baseline case with a positive mass prior, the extrapolation framework restricted to a positive prior, and the full implementation utilizing a negative prior.

When we analyze the case of a dynamical DE we use the CPL parametrization that adds two extra parameters,  $w_0$  and  $w_a$ . For each DE model, one run was performed with fixed neutrino mass and another with varying neutrino mass. When  $\sum m_\nu$  is sampled, we assume three degenerate mass eigenstates while in the opposite case  $\sum m_\nu$  is fixed to a value of 0.06 eV assuming a single non-zero mass neutrino.

In Table II are presented the priors used for each parameter, following those of the DESI collaboration [13].

Model	Parameter	Prior
$\Lambda$ CDM	$\omega_{cdm}$	$\mathcal{U}[0.001, 0.99]$
	$\omega_b$	$\mathcal{U}[0.005, 0.1]$
	$100\theta_*$	$\mathcal{U}[0.5, 10]$
	$\ln(10^{10} A_s)$	$\mathcal{U}[1.61, 3.91]$
	$n_s$	$\mathcal{U}[0.8, 1.2]$
	$\Omega_k$	$\mathcal{U}[-0.3, 0.3]$
	$\tau$	$\mathcal{U}[0.01, 0.8]$
CPL DE	$\omega_0$	$\mathcal{U}[-3, 1]$
	$\omega_a$	$\mathcal{U}[-3, 2]$
Adding Neutrinos	$\sum m_\nu$	$\mathcal{U}[0, 5]$
	$\sum m_{\nu,eff}$	$\mathcal{U}[-5, 5]$

TABLE II: Set of parameters and their respective priors used in the analysis. Notice that all priors are flat priors in order to let MCMC explore an extensive configuration space for the models.

## IV. RESULTS

This section presents the results obtained from the cosmological inference process. The discussion is organized into three subsections: Section IV A details the findings for the standard  $\Lambda$ CDM model, assuming a positive neutrino mass prior; the same goes for Section IV B, but here the CPL dynamical dark energy model is adopted. Section IV C provides the outcomes obtained when the negative neutrino mass regime is explored for both DE models. Additionally, Section IV D presents various goodness-of-fit criteria obtained via `iminuit`, which is used to evaluate model performance and to determine the statistical preference for each model.

### A. $\Lambda$ CDM model

First, we present the results for the  $\Lambda$ CDM model. Figure 2 displays the 2D posterior contours for selected parameters, comparing the  $\Lambda$ CDM model in both spatially flat and non-flat scenarios. As illustrated, the inclusion of spatial curvature shifts  $\sum m_\nu$  to larger positive values, improving the constraints on the neutrino mass sum, a result consistent with the findings in Ref. [16]. When  $\Omega_k$  is treated as a free parameter, the resulting bound is

$$\Lambda\text{CDM}+\Omega_k : \sum m_\nu < 0.135 \text{ (95\%)}. \quad (9)$$

As expected, allowing  $\Omega_k$  to vary impacts the estimation of  $\Omega_m$  which in turn indirectly influences the neutrino mass constraints due to the geometric degeneracy. Regarding the spatial curvature, while the neutrino mass is fixed, we find a  $2.15\sigma$  deviation from a flat Universe. However, when the neutrino mass is also varied, this statistical significance relaxes to  $1.65\sigma$  from the flat model.

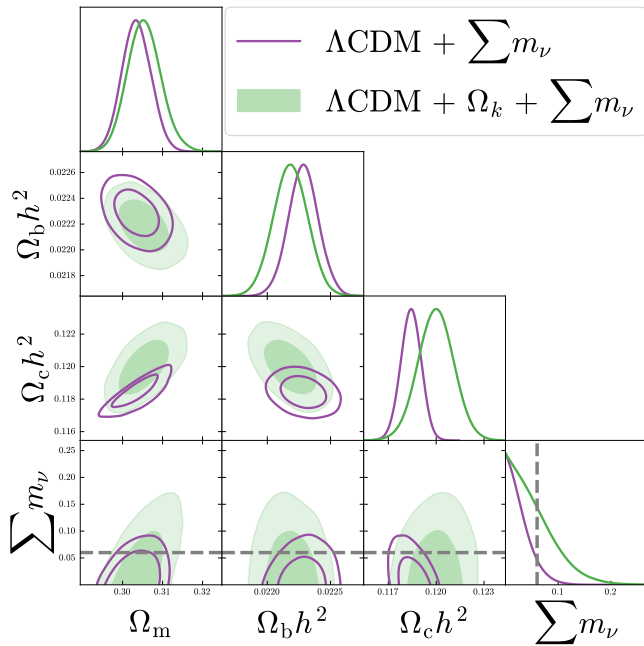


FIG. 2: Triangular plot showing the confidence contours for the  $\Lambda\text{CDM} + \sum m_\nu$  (purple) versus the  $\Lambda\text{CDM} + \Omega_k + \sum m_\nu$  (green) models. As observed, including curvature as a varying parameter affects  $\Omega_m$ , causing the associated densities  $\Omega_b$ ,  $\Omega_{cdm}$  and  $\Omega_\nu$  to be affected as well. The grey dashed line corresponds to the lower bound value  $\sum m_\nu = 0.06$  eV.

### B. $\omega_0\omega_a$ CDM Model

Motivated by the recent DESI results [12, 26, 55, 56] favoring a dynamical dark energy scenario, we extend our analysis to include the  $\omega_0\omega_a$ CDM model. In this scenario, the difference between the flat Universe case and the one with curvature is not as noticeable as it is in the  $\Lambda$ CDM model, as we can see in the Figure 3. Even so, the neutrino mass constraint is relaxed relative to the flat case case, yielding a value of

$$\omega_0\omega_a\text{CDM} + \Omega_k : \sum m_\nu < 0.171 \quad (95\%) \quad (10)$$

In this case, the presence of curvature affects the  $\omega_0$  and  $\omega_a$  parameters; as seen in Figure 4. It is clear that curvature reduces the tension found in the  $\Lambda$ CDM model (this being the case for  $\omega_0 = -1$  and  $\omega_a = 0$ ).

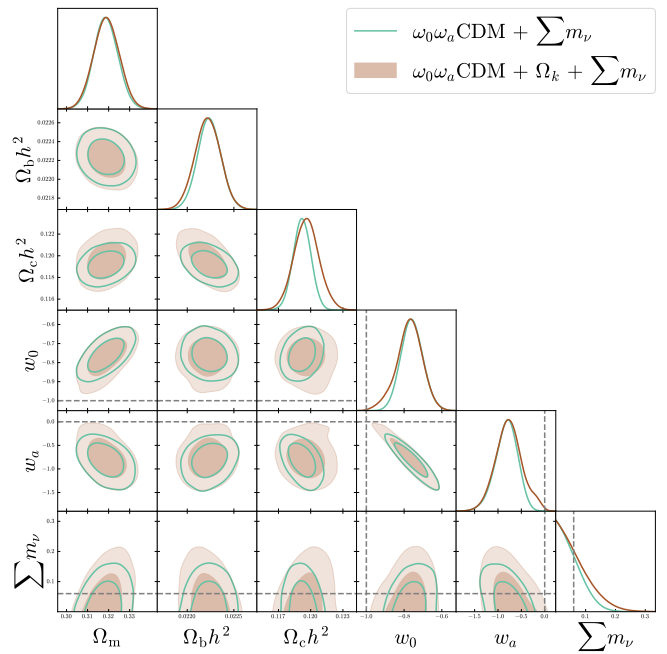


FIG. 3: Triangular plot showing the confidence contours for  $\omega_0\omega_a\text{CDM} + \sum m_\nu$  (lime) against  $\omega_0\omega_a\text{CDM} + \Omega_k + \sum m_\nu$  (brown). No significant shift is observed in the  $\Omega_m$  posterior, whereas  $\Omega_c$  and  $\sum m_\nu$  show a slight sensitivity to the inclusion of curvature, with the effect being more pronounced for the former.

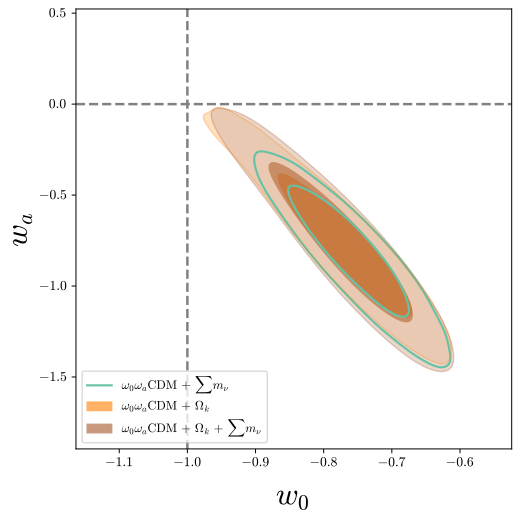


FIG. 4: 2D plot of the  $\omega_0$  and  $\omega_a$  parameters. It can be observed that the contours for the  $\omega_0\omega_a\text{CDM} + \Omega_k$  and  $\omega_0\omega_a\text{CDM} + \Omega_k + \sum m_\nu$  models are nearly identical, while showing a significant difference from  $\omega_0\omega_a\text{CDM} + \sum m_\nu$ ; this clearly indicates that the shift is driven entirely by curvature. However, the 68% C.L. contour is quite similar across the three models, with the statistical deviation becoming apparent at the 95% C.L., as clearly shown in Figure 3.

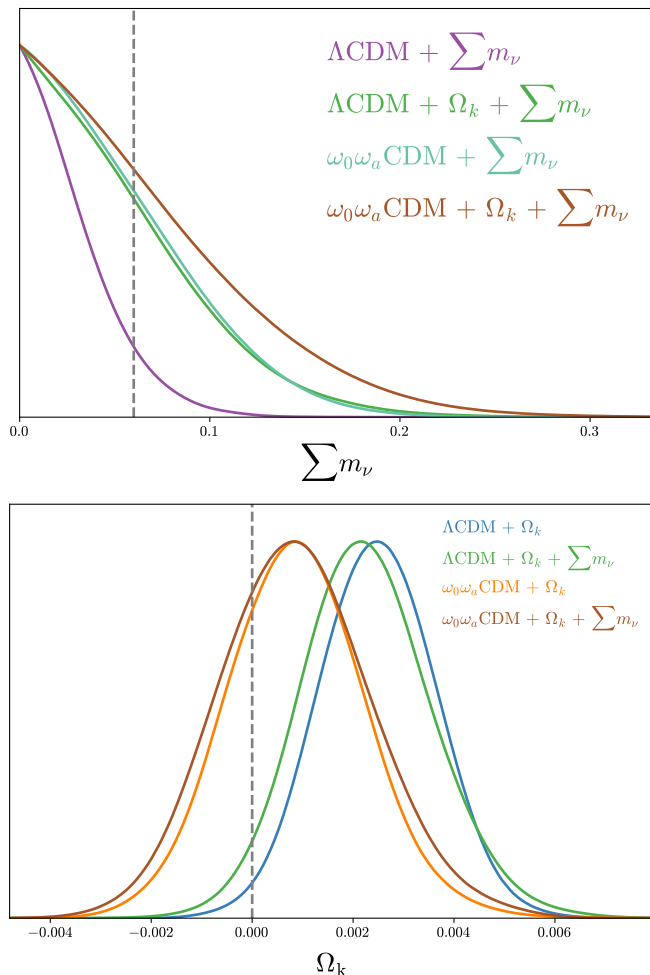


FIG. 5: (**Upper**) 1D posterior distribution for  $\sum m_\nu$  across different models. (**Lower**) 1D posterior distribution for  $\Omega_k$  across different models. The vertical dashed lines indicate  $\sum m_\nu = 0.06$  eV and  $\Omega_k = 0$ , respectively.

The next step is to compare the  $\Lambda$ CDM results with those of the  $\omega_0\omega_a$ CDM model. Figure 5 shows the posterior distributions for  $\sum m_\nu$  and  $\Omega_k$ . Note that all posteriors of  $\sum m_\nu$  (upper panel) tend to peak near its lower limit, suggesting that they lie at negative values; however, the presence of curvature seems to alleviate this trend. Also interesting in the upper panel is to note that the posteriors for  $\Lambda$ CDM +  $\Omega_k$  +  $\sum m_\nu$  and  $\omega_0\omega_a$ CDM +  $\sum m_\nu$  are nearly identical, demonstrating that the former achieves the same improvement as the latter with one fewer parameter. Concerning  $\Omega_k$  (lower panel), both models exhibit a preference for a positive value, echoing the findings in [16], which show that the relationship between  $\sum m_\nu$  and  $\Omega_k$  is not bilateral, as curvature affects the neutrino mass, but the reverse is not true in the same proportion.

The upper panel of Figure 5 shows that these models are unable to resolve the issue of the  $\sum m_\nu$  posterior peak being located at positive values; instead, the distributions suggest a trend toward negative values. Since these posteriors are non-Gaussian, it is not possible to determine whether the shift observed when including curvature or switching models is physically motivated or a statistical artifact arising from the additional parameters. To explore this, we widen the prior to include the negative mass region. We performed additional runs following the methodology described above. Table III shows our best-fit results for the main cosmological parameters, whereas in Appendix V we display the complete results for all sampled parameters across the analyzed models.

### C. Effective neutrino mass results

A particle with negative mass is physically meaningless. However, in our context, it serves as a means to explore a new parameter space which, as suggested in Figure 5, is statistically preferred by the data. Figure 7 presents triangular plots for the four analyzed models, comparing them with their counterparts that are subject to positive priors. It is clear that extending the parameter space to include negative masses preserves the inherent degeneracies of the neutrino mass sum, while the transition between these regimes remains smooth. Note that all posteriors that include negative mass priors peak at the negative mass range. This clearly seen in Figure 6 that summarizes the 1D probability behavior of  $\sum m_{\nu,eff}$  across all cases. The white region, corresponding to a positive neutrino mass, yields results equivalent to those shown in the upper panel of Figure 5. However, as previously noted, the most interesting and complementary insights emerge in the region where  $\sum m_\nu < 0$ . The posterior for the  $\omega_0\omega_a$ CDM +  $\Omega_k$  +  $\sum m_{\nu,eff}$  model exhibits a larger standard deviation, and hence, yielding a larger positive mass area; nevertheless, the peak of this distribution is shifted further away from the lower bound of the neutrino mass sum. The  $\Lambda$ CDM +  $\sum m_{\nu,eff}$  model appears to exhibit the poorest performance, showing a  $2.59\sigma$  tension relative to the value  $\sum m_\nu = 0.06$  eV. Conversely, the  $\Lambda$ CDM +  $\Omega_k$  +  $\sum m_{\nu,eff}$  model shows a better performance, yielding a tension of  $1.17\sigma$  with respect to the same value. Regarding the  $\omega_0\omega_a$ CDM models,  $\omega_0\omega_a$ CDM +  $\sum m_{\nu,eff}$  shows a  $1.18\sigma$  tension while  $\omega_0\omega_a$ CDM +  $\Omega_k$  +  $\sum m_{\nu,eff}$  can reduce it to  $1.13\sigma$  losing estimation power in exchange.

Model	$\Omega_m$	$10^3\Omega_k$	$\sum m_\nu$ [eV]	$\omega_0$	$\omega_a$
$\Lambda$ CDM	$0.3049 \pm 0.0036$	-	-	-	-
$\Lambda$ CDM + $\sum m_\nu$	$0.3035 \pm 0.0036$	-	$< 0.0731$	-	-
$\Lambda$ CDM + $\Omega_k$	$0.3058 \pm 0.0036$	$2.5 \pm 1.2$	-	-	-
$\Lambda$ CDM + $\Omega_k$ + $\sum m_\nu$	$0.3055^{+0.0039}_{-0.0044}$	$2.3^{+1.2}_{-1.4}$	$< 0.135$	-	-
$\omega_0\omega_a$ CDM + $\sum m_\nu$	$0.3187 \pm 0.0057$	-	$< 0.130$	$-0.758 \pm 0.059$	$-0.82^{+0.26}_{-0.21}$
$\omega_0\omega_a$ CDM + $\Omega_k$	$0.3187 \pm 0.0059$	$0.9 \pm 1.4$	-	$-0.774^{+0.073}_{-0.057}$	$-0.76^{+0.23}_{-0.29}$
$\omega_0\omega_a$ CDM + $\Omega_k$ + $\sum m_\nu$	$0.3190 \pm 0.0061$	$0.9^{+1.4}_{-1.6}$	$< 0.171$	$-0.773^{+0.074}_{-0.060}$	$-0.76^{+0.26}_{-0.30}$
$\Lambda$ CDM + $\sum m_{\nu,\text{eff}}$	$0.2992 \pm 0.0045$	-	$-0.073^{+0.051}_{-0.064}$	-	-
$\Lambda$ CDM + $\Omega_k$ + $\sum m_{\nu,\text{eff}}$	$0.3013 \pm 0.0054$	$1.1^{+1.5}_{-1.7}$	$-0.011^{+0.052}_{-0.050}$	-	-
$\omega_0\omega_a$ CDM + $\sum m_{\nu,\text{eff}}$	$0.3156 \pm 0.0063$	-	$-0.052^{+0.095}_{-0.084}$	$-0.787 \pm 0.061$	$-0.63^{+0.29}_{-0.26}$
$\omega_0\omega_a$ CDM + $\Omega_k$ + $\sum m_{\nu,\text{eff}}$	$0.3146 \pm 0.0071$	$-0.6^{+1.6}_{-1.9}$	$-0.07 \pm 0.11$	$-0.786 \pm 0.061$	$-0.61^{+0.29}_{-0.26}$

TABLE III: Key cosmological parameter constraints. Results represent the 68% C.L. intervals, except for the sum of neutrino masses, which is quoted at the 95% C.L. Regarding the results for the  $\omega_0\omega_a$ CDM +  $\sum m_\nu$  model, the analysis utilizes the publicly available MCMC chains provided by the DESI collaboration as part of their Data Release 2 (DR2) [12].

A particle with negative mass is physically meaningless. However, in our context, it serves as a means to explore a new parameter space which, as suggested in Figure 5, is statistically preferred by the data. Figure 7 presents triangular plots for the four analyzed models, comparing them with their counterparts that are subject to positive priors. It is clear that extending the parameter space to include negative masses preserves the inherent degeneracies of the neutrino mass sum, while the transition between these regimes remains smooth. Note that all posteriors that include negative mass priors peak at the negative mass range. This clearly seen in Figure 6 that summarizes the 1D probability behavior of  $\sum m_{\nu,\text{eff}}$  across all cases. The white region, corresponding to a positive neutrino mass, yields results equivalent to those shown in the upper panel of Figure 5. However, as previously noted, the most interesting and complementary insights emerge in the region where  $\sum m_\nu < 0$ . The posterior for the  $\omega_0\omega_a$ CDM+ $\Omega_k$ + $\sum m_{\nu,\text{eff}}$  model exhibits a larger standard deviation, and hence, yielding a larger positive mass area; nevertheless, the peak of this distribution is shifted further away from the lower bound of the neutrino mass sum. The  $\Lambda$ CDM +  $\sum m_{\nu,\text{eff}}$  model appears to exhibit the poorest performance, showing a  $2.59\sigma$  tension relative to the value  $\sum m_\nu = 0.06$  eV. Conversely, the  $\Lambda$ CDM +  $\Omega_k$  +  $\sum m_{\nu,\text{eff}}$  model shows a better performance, yielding a tension of  $1.17\sigma$  with respect to the same value. Regarding the  $\omega_0\omega_a$ CDM models,  $\omega_0\omega_a$ CDM +  $\sum m_{\nu,\text{eff}}$  shows a  $1.18\sigma$  tension while  $\omega_0\omega_a$ CDM +  $\Omega_k$  +  $\sum m_{\nu,\text{eff}}$  can reduce it to  $1.13\sigma$  loosening estimation power in exchange.

As shown in Appendix A, the constraints on  $\sum m_\nu$  are insensitive to the updated reanalysis for the DESY5 dataset. This reinforces the overall robustness of the findings presented above.

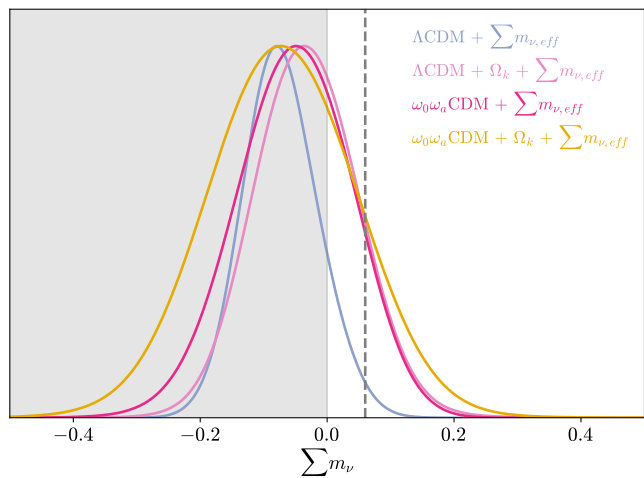


FIG. 6: 1D posterior distributions for the effective neutrino mass sum,  $\sum m_{\nu,\text{eff}}$ . Interestingly, while the behavior in the positive region remains consistent with results obtained under a strictly positive prior, the distribution peaks in the negative mass range indicate that the  $\Lambda$ CDM+ $\Omega_k$ + $\sum m_{\nu,\text{eff}}$  model exhibits the best performance. Once again, we observe that the neutrino mass constraints for the  $\Lambda$ CDM+ $\Omega_k$ + $\sum m_{\nu,\text{eff}}$  and  $\omega_0\omega_a$ CDM+ $\sum m_{\nu,\text{eff}}$  models are remarkably similar. The vertical dashed line denotes the value of  $\sum m_\nu = 0.06$  eV, and the grey shaded area highlights the negative mass region.

#### D. Goodness of fit

To evaluate model performance beyond parameter estimation alone and to determine the goodness-of-fit to the data, we computed several statistical metrics based on the results obtained from the `iminuit` optimizer. Specifically, we report the  $\Delta\chi^2_{MAP}$ , the Akaike Information

Criterion (AIC), and the Bayesian Information Criterion (BIC), all based on the maximum likelihood; additionally, we provide the Deviance Information Criterion (DIC) derived from the posterior samples, following the standard methodology described in Ref. [57].

First, the fit is assessed via the Maximum a Posteriori (MAP) estimate, quantified by the log-likelihood difference  $\Delta\chi_{MAP}^2 \equiv -2\Delta\ln\mathcal{L}$ . To compare the relative performance of models with varying complexities, we employ the AIC, defined as:

$$AIC \equiv \chi^2 + 2k, \quad (11)$$

where  $k$  denotes the number of free parameters.

Additionally, we consider the BIC, which accounts for the total number of data points  $N$  in its penalty term:

$$BIC \equiv \chi^2 + k \ln N. \quad (12)$$

Finally, the DIC is utilized to leverage the full posterior information provided by the MCMC chains. A key step in this calculation is defining the effective number of model parameters,  $p_D$ . In this work, we specifically adopt the alternative form for this quantity by setting  $\chi^2(\bar{\theta}) = \chi_{min}^2(\theta)$ , which yields:

$$p_D \equiv \overline{\chi^2(\theta)} - \chi_{min}^2(\theta), \quad (13)$$

that leads to the expression:

$$DIC \equiv 2\overline{\chi^2(\theta)} - \chi_{min}^2(\theta). \quad (14)$$

Table IV summarizes the goodness-of-fit metrics for each established criterion, using  $\Lambda$ CDM as the reference model. We computed  $\Delta X = X_{model} - X_{\Lambda CDM}$ , where  $X$  is the chosen criteria and  $X_{\Lambda CDM}$  correspond to the criteria value for the minimal  $\Lambda$ CDM model. Regarding the  $\Delta\chi_{MAP}^2$  values, the  $\omega_0\omega_a$ CDM model and its extensions, as expected, yield improved fits due to the additional degrees of freedom provided by their extra parameters. In all cases, a lower value for these criteria indicates a superior model fit. Interestingly, a counterintuitive trend emerges when allowing for negative neutrino mass cases: the  $\chi^2$  values increase compared to the strictly positive mass cases, despite the data showing a preference for this negative region. This discrepancy likely suggests that exploring this portion of the parameter space induces global shifts in other cosmological parameters, affecting the overall fit quality.

Furthermore, the  $\Delta AIC$  results indicate a significant improvement for the  $\omega_0\omega_a$ CDM models with fixed neutrino mass relative to  $\Lambda$ CDM. Conversely, the  $\Delta BIC$  values show the opposite trend, as this criterion imposes a more stringent penalty on model complexity. Finally, the  $\Delta DIC$  results are less pronounced but consistently favor the  $\omega_0\omega_a$ CDM framework. This leads us to conclude that the increased flexibility of this model allows for a more robust alignment with the data, even after accounting for the effective number of parameters.

Model	$\Delta\chi_{MAP}^2$	$\Delta AIC$	$\Delta BIC$	$\Delta DIC$
$\Lambda$ CDM + $\Omega_k$	-6.59	-4.59	2.61	-3.01
$\Lambda$ CDM + $\sum m_\nu$	-1.04	0.96	8.16	4.03
$\Lambda$ CDM + $\sum m_{\nu,eff}$	-0.56	1.44	8.65	1.91
$\Lambda$ CDM + $\Omega_k + \sum m_\nu$	-3.98	0.02	14.43	1.64
$\Lambda$ CDM + $\Omega_k + \sum m_{\nu,eff}$	-1.65	2.35	16.76	1.47
$\omega_0\omega_a$ CDM	-14.81	-10.81	3.60	-
$\omega_0\omega_a$ CDM + $\Omega_k$	-16.54	-10.54	11.08	-6.69
$\omega_0\omega_a$ CDM + $\sum m_\nu$	-13.69	-7.69	13.93	-4.01
$\omega_0\omega_a$ CDM + $\sum m_{\nu,eff}$	-10.22	-4.22	17.40	-5.68
$\omega_0\omega_a$ CDM + $\Omega_k + \sum m_\nu$	-14.24	-6.24	22.59	-3.79
$\omega_0\omega_a$ CDM + $\Omega_k + \sum m_{\nu,eff}$	-12.99	-4.99	23.84	-3.83

TABLE IV: Comparison of statistical criteria relative to the  $\Lambda$ CDM model as reference. Differences are calculated as  $\Delta X = X_{model} - X_{\Lambda CDM}$ .

## V. CONCLUSIONS

The  $\Lambda$ CDM model remains under constant scrutiny in the current era of precision cosmology, facing significant challenges such as the treated here, i.e. the apparent discrepancy between cosmological upper bounds on the neutrino mass sum and the lower limits established by terrestrial oscillations experiments. The primary objective of this work was to analyze the impact of spatial curvature on neutrino mass constraints by exploring the degeneracies within the parameter space. To this end, we employed the latest CMB, BAO, and SNe Ia datasets to perform a Bayesian parameter estimation for the  $\Lambda$ CDM and  $\omega_0\omega_a$ CDM models, alongside their respective extensions including  $\Omega_k$  and  $\sum m_\nu$ . This analysis included an exploration of the parameter space where the neutrino mass takes negative effective values, allowing for a deeper evaluation of the trends observed in the data.

In the scenario where a strictly positive neutrino mass was imposed, our results are consistent with previous literature. The inclusion of spatial curvature as a free parameter shows a perceived reduction in the tension with terrestrial measurements for the  $\Lambda$ CDM model. This effect is comparable to that observed when shifting toward a dynamical dark energy equation of state, as illustrated in the upper panel of Figure 5. However, since the resulting posteriors in these models exhibit a strong truncation at  $\sum m_\nu = 0$  and a marked departure from Gaussianity, it is not possible to quantify this tension through conventional  $\sigma$  standard deviation method. Consequently, one cannot determine whether the observed reduction in tension represents a physical convergence toward the experimental minimal value, 0.06 eV, or is merely a consequence of the loss in constraining power as the model complexity increases. This statistical ambiguity is precisely what motivates the shift toward the negative effective mass scenario.

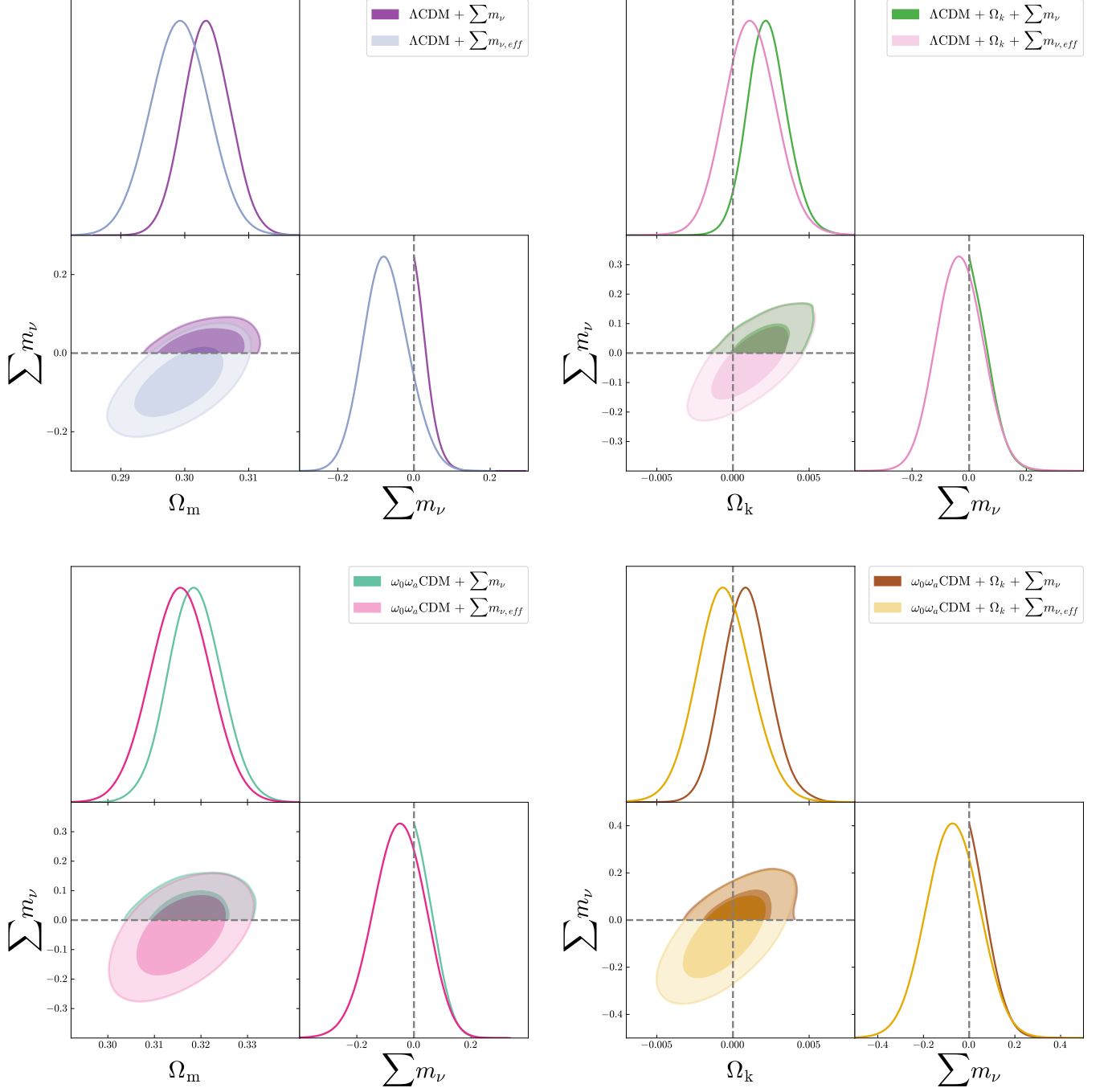


FIG. 7: Illustrative posterior distribution for the four analyzed scenarios. The smooth behavior of the contours across the different panels reflects the preference for the negative mass regime and the robustness of the sampling process. Notably, the characteristic degeneracies between cosmological parameters are consistently maintained throughout the various models extensions, confirming that the physical correlations remain stable even as the parameter space is expanded.

To address this issue, we modified the communication interface between the Boltzmann code (CLASS) and the sampler (Cobaya), enabling an agnostic exploration of the mass sign. A key highlight of the results presented in Figure 7 is the existence of a smooth transition in the posteriors between the positive and negative mass regimes. This continuity underscores that allowing  $\sum m_\nu < 0$  is the statistically correct approach for these datasets; otherwise, the parameter space is artificially constrained, introducing biases due to boundary effects in the estimates. From our results, we observe that curvature reduces the tension relative to the 0.06 eV value, bringing it down from  $2.59\sigma$ , given  $\sum m_{\nu,eff} = -0.073^{+0.051}_{-0.064}$  in the  $\Lambda\text{CDM} + \sum m_{\nu,eff}$  model, to  $1.17\sigma$  with  $\sum m_{\nu,eff} = -0.011^{+0.052}_{-0.050}$  within the  $\Lambda\text{CDM} + \Omega_k + \sum m_{\nu,eff}$  model. While this trend persists in the  $\omega_0\omega_a\text{CDM} + \sum m_{\nu,eff}$  model, the increased number of free parameters degrades the overall constraining power. Analysis of the various goodness-of-fit criteria, with the exception of the BIC, reveals a general trend where the  $\omega_0\omega_a\text{CDM}$  model and its extensions provide a better fit due to their greater parametric flexibility, though this does not inherently resolve the data's preference for null or negative mass values. The BIC criteria that penalize the number of free parameters favors the  $\Lambda\text{CDM}$  models over their respective  $\omega_0\omega_a\text{CDM}$  counterparts. Now, models  $\Lambda\text{CDM} + \Omega_k + \sum m_\nu$  and  $\omega_0\omega_a\text{CDM} + \sum m_\nu$  are quite similar with a little preference for the later.

The recent trend of questioning the validity of the standard model, largely driven by the DESI results, has initiated a period of intense activity in modern cosmology. Our findings suggest that the use of negative effective masses should not be viewed as a mere mathematical curiosity but should be established as a new diagnostic standard in cosmological parameter analysis. This practice allows for the identification of prior-driven biases and ensures that conclusions regarding the nature of neutrinos are not artifacts of an arbitrary delimitation of the parameter space. In a landscape where tensions between CMB, BAO, and SNe Ia datasets suggest possible departures from  $\Lambda\text{CDM}$ , adopting methodologies that are agnostic to physical boundaries is fundamental to determining whether we are witnessing new physics or statistical fluctuations at the limit of our current precision.

## VI. ACKNOWLEDGMENTS

The authors acknowledge support by SECIHTI (CONAHCyT) project CBF2023-2024-589. H. P-H acknowledges support from SECIHTI (CONAHCyT) through the doctoral scholarship, CVU No. 1182916.

This research used data obtained with the Dark Energy Spectroscopic Instrument (DESI). DESI construction and operations is managed by the Lawrence Berkeley National Laboratory. This material is based upon work supported by the U.S. Department of Energy, Office of Science, Office of High-Energy Physics, un-

der Contract No. DE-AC02-05CH11231, and by the National Energy Research Scientific Computing Center, a DOE Office of Science User Facility under the same contract. Additional support for DESI was provided by the U.S. National Science Foundation (NSF), Division of Astronomical Sciences under Contract No. AST-0950945 to the NSF's National Optical-Infrared Astronomy Research Laboratory; the Science and Technology Facilities Council of the United Kingdom; the Gordon and Betty Moore Foundation; the Heising-Simons Foundation; the French Alternative Energies and Atomic Energy Commission (CEA); the National Council of Humanities, Science and Technology of Mexico (CONAHCYT); the Ministry of Science and Innovation of Spain (MICINN), and by the DESI Member Institutions: [www.desi.lbl.gov/collaborating-institutions](http://www.desi.lbl.gov/collaborating-institutions). The DESI collaboration is honored to be permitted to conduct scientific research on I'oligam Du'ag (Kitt Peak), a mountain with particular significance to the Tohono O'odham Nation. Any opinions, findings, and conclusions or recommendations expressed in this material are those of the author(s) and do not necessarily reflect the views of the U.S. National Science Foundation, the U.S. Department of Energy, or any of the listed funding agencies.

- 
- [1] I. Esteban, M. C. Gonzalez-Garcia, M. Maltoni, I. Martinez-Soler, J. P. Pinheiro, and T. Schwetz, *Journal of High Energy Physics* **2024** (2024), ISSN 1029-8479, URL [http://dx.doi.org/10.1007/JHEP12\(2024\)216](http://dx.doi.org/10.1007/JHEP12(2024)216).
- [2] M. Aker, K. Altenmüller, M. Arenz, M. Babutzka, J. Barrett, S. Bauer, M. Beck, A. Beglarian, J. Behrens, T. Bergmann, et al. (KATRIN Collaboration), *Phys. Rev. Lett.* **123**, 221802 (2019), URL <https://link.aps.org/doi/10.1103/PhysRevLett.123.221802>.
- [3] M. Aker et al. (KATRIN), *Nature Phys.* **18**, 160 (2022), 2105.08533.
- [4] K. Collaboration†, M. Aker, D. Batzler, A. Beglarian, J. Behrens, J. Beisenkötter, M. Biassoni, B. Bieringer, Y. Biondi, F. Block, et al., *Science* **388**, 180 (2025), <https://www.science.org/doi/pdf/10.1126/science.adq9592>, URL <https://www.science.org/doi/abs/10.1126/science.adq9592>.
- [5] S. S. Gershtein and Y. B. Zeldovich, *JETP Lett.* **4**, 120 (1966).
- [6] R. A. C. Croft, W. Hu, and R. Davé, *Physical Review Letters* **83**, 1092–1095 (1999), ISSN 1079-7114, URL <http://dx.doi.org/10.1103/PhysRevLett.83.1092>.
- [7] P. A. R. Ade et al. (Planck), *Astron. Astrophys.* **566**, A54 (2014), 1311.1657.
- [8] N. Palanque-Delabrouille, C. Yèche, J. Baur, C. Magneville, G. Rossi, J. Lesgourgues, A. Borde, E. Burtin, J.-M. LeGoff, J. Rich, et al., *Journal of Cosmology and Astroparticle Physics* **2015**, 011–011 (2015), ISSN 1475-7516, URL <http://dx.doi.org/10.1088/1475-7516/2015/11/011>.
- [9] S. Alam, M. Aubert, S. Avila, C. Balland, J. E. Bautista, M. A. Bershad, D. Bizyaev, M. R. Blanton, A. S. Bolton, J. Bovy, et al., *Physical Review D* **103** (2021), ISSN 2470-0029, URL <http://dx.doi.org/10.1103/PhysRevD.103.083533>.
- [10] S. Aiola, E. Calabrese, L. Maurin, S. Naess, B. L. Schmitt, M. H. Abitbol, G. E. Addison, P. A. R. Ade, D. Alonso, M. Amiri, et al., *Journal of Cosmology and Astroparticle Physics* **2020**, 047–047 (2020), ISSN 1475-7516, URL <http://dx.doi.org/10.1088/1475-7516/2020/12/047>.
- [11] E. Di Valentino, W. Giarè, A. Melchiorri, and J. Silk, *Physical Review D* **106** (2022), ISSN 2470-0029, URL <http://dx.doi.org/10.1103/PhysRevD.106.103506>.
- [12] M. Abdul Karim, J. Aguilar, S. Ahlen, S. Alam, L. Allen, C. A. Prieto, O. Alves, A. Anand, U. Andrade, E. Armengaud, et al., *Phys. Rev. D* **112**, 083515 (2025), 2503.14738.
- [13] W. Elbers, A. Aviles, H. E. Noriega, D. Chebat, A. Menegas, C. S. Frenk, C. Garcia-Quintero, D. Gonzalez, M. Ishak, O. Lahav, et al. (DESI Collaboration), *Phys. Rev. D* **112**, 083513 (2025), URL <https://link.aps.org/doi/10.1103/w9pk-xsk7>.
- [14] M. Chevallier and D. Polarski, *Int. J. Mod. Phys. D* **10**, 213 (2001), gr-qc/0009008.
- [15] E. V. Linder, *Physical Review Letters* **90** (2003), ISSN 1079-7114, URL <http://dx.doi.org/10.1103/PhysRevLett.90.091301>.
- [16] S.-F. Chen and M. Zaldarriaga, *Journal of Cosmology and Astroparticle Physics* **2025**, 014 (2025), URL <https://doi.org/10.1088/1475-7516/2025/08/014>.
- [17] W. Elbers, C. S. Frenk, A. Jenkins, B. Li, and S. Pascoli, *Phys. Rev. D* **111**, 063534 (2025), 2407.10965.
- [18] P. F. de Salas, D. V. Forero, S. Gariazzo, P. Martínez-Miravé, O. Mena, C. A. Ternes, M. Tórtola, and J. W. F. Valle, *Journal of High Energy Physics* **2021** (2021), ISSN 1029-8479, URL [http://dx.doi.org/10.1007/JHEP02\(2021\)071](http://dx.doi.org/10.1007/JHEP02(2021)071).
- [19] F. Capozzi, E. Di Valentino, E. Lisi, A. Marrone, A. Melchiorri, and A. Palazzo, *Phys. Rev. D* **104**, 083031 (2021), 2107.00532.
- [20] E. Calabrese, J. C. Hill, H. T. Jense, A. La Posta, I. Abril-Cabezas, G. E. Addison, P. A. Ade, S. Aiola, T. Alford, D. Alonso, et al., *Journal of Cosmology and Astroparticle Physics* **2025**, 063 (2025), URL <https://doi.org/10.1088/1475-7516/2025/11/063>.
- [21] M. Loverde and Z. J. Weiner, *Journal of Cosmology and Astroparticle Physics* **2024**, 048 (2024), ISSN 1475-7516, URL <http://dx.doi.org/10.1088/1475-7516/2024/12/048>.
- [22] D. W. Hogg (2000), astro-ph/9905116, URL <https://arxiv.org/abs/astro-ph/9905116>.
- [23] M. Shoji and E. Komatsu, *Phys. Rev. D* **81**, 123516 (2010), URL <https://link.aps.org/doi/10.1103/PhysRevD.81.123516>.
- [24] J. Lesgourgues and S. Pastor, *Advances in High Energy Physics* **2012**, 1–34 (2012), ISSN 1687-7365, URL <http://dx.doi.org/10.1155/2012/608515>.
- [25] N. Aghanim, Y. Akrami, M. Ashdown, J. Aumont, C. Baccigalupi, M. Ballardini, A. J. Banday, R. B. Barreiro, N. Bartolo, S. Basak, et al., *Astronomy & Astrophysics* **641**, A5 (2020), ISSN 1432-0746, URL <http://dx.doi.org/10.1051/0004-6361/201936386>.
- [26] DES Collaboration, T. M. C. Abbott, M. Acevedo, M. Aguena, A. Alarcon, S. Allam, O. Alves, A. Amon, F. Andrade-Oliveira, J. Annis, et al., *Astrophys. J. Lett.* **973**, L14 (2024), 2401.02929.
- [27] D. Brout, D. Scolnic, B. Popovic, A. G. Riess, A. Carr, J. Zuntz, R. Kessler, T. M. Davis, S. Hinton, D. Jones, et al., *The Astrophysical Journal* **938**, 110 (2022), ISSN 1538-4357, URL <http://dx.doi.org/10.3847/1538-4357/ac8e04>.
- [28] D. Rubin, G. Aldering, M. Betoule, A. Fruchter, X. Huang, A. G. Kim, C. Lidman, E. Linder, S. Perlmutter, P. Ruiz-Lapuente, et al., *The Astrophysical Journal* **986**, 231 (2025), URL <https://doi.org/10.3847/1538-4357/adc0a5>.
- [29] A. Chudaykin, M. M. Ivanov, and O. H. E. Philcox (2026), 2602.18554.
- [30] G.-H. Du, T.-N. Li, P.-J. Wu, J.-F. Zhang, and X. Zhang, arXiv e-prints arXiv:2507.16589 (2025), 2507.16589.
- [31] S. Ahlen, A. Aviles, B. Cartwright, K. Croker, W. Elbers, D. Farrah, N. Fernandez, G. Niz, J. Rohlf, G. Tarlé, et al., *Physical Review Letters* **135** (2025), ISSN 1079-7114.
- [32] F. J. Qu, K. M. Surrao, B. Bolliet, J. C. Hill, B. D. Sherwin, H. T. Jense, and A. La Posta, *Phys. Rev. D* **111**, 123507 (2025), URL <https://link.aps.org/doi/10.1103/xhh6-9v62>.
- [33] H. García Escudero, S. H. Mirpoorian, and L. Pogossian, *The Astrophysical Journal Letters* **998**, L41 (2026), URL <https://doi.org/10.3847/2041-8213/ae40bf>.
- [34] R. K. Sharma and J. Lesgourgues, *Journal of Cosmology*

- and *Astroparticle Physics* **2026**, 034 (2026), URL <https://doi.org/10.1088/1475-7516/2026/02/034>.
- [35] N. Sailer, G. S. Farren, S. Ferraro, and M. White, *Phys. Rev. Lett.* **136**, 081002 (2026), URL <https://link.aps.org/doi/10.1103/6r54-81v4>.
- [36] J. Torrado and A. Lewis, *Journal of Cosmology and Astroparticle Physics* **2021**, 057 (2021), ISSN 1475-7516, URL <http://dx.doi.org/10.1088/1475-7516/2021/05/057>.
- [37] J. Torrado and A. Lewis, *Cobaya: Bayesian analysis in cosmology*, Astrophysics Source Code Library, record ascl:1910.019 (2019).
- [38] A. Lewis, A. Challinor, and A. Lasenby, *The Astrophysical Journal* **538**, 473–476 (2000), ISSN 1538-4357, URL <http://dx.doi.org/10.1086/309179>.
- [39] D. Blas, J. Lesgourgues, and T. Tram, *Journal of Cosmology and Astroparticle Physics* **2011**, 034–034 (2011), ISSN 1475-7516, URL <http://dx.doi.org/10.1088/1475-7516/2011/07/034>.
- [40] J. Lesgourgues and T. Tram, *Journal of Cosmology and Astroparticle Physics* **2011**, 032–032 (2011), ISSN 1475-7516, URL <http://dx.doi.org/10.1088/1475-7516/2011/09/032>.
- [41] A. Gelman and D. B. Rubin, *Statistical Science* **7**, 457 (1992), URL <https://doi.org/10.1214/ss/1177011136>.
- [42] A. Lewis, *JCAP* **08**, 025 (2025), 1910.13970.
- [43] N. Craig, D. Green, J. Meyers, and S. Rajendran, *JHEP* **09**, 097 (2024), 2405.00836.
- [44] D. Naredo-Tuero, M. Escudero, E. Fernandez-Martinez, X. Marcano, and V. Poulin, *Phys. Rev. D* **110**, 123537 (2024), URL <https://link.aps.org/doi/10.1103/PhysRevD.110.123537>.
- [45] C.-P. Ma and E. Bertschinger, *Astrophys. J.* **455**, 7 (1995), astro-ph/9506072.
- [46] E. Rosenberg, S. Gratton, and G. Efstathiou, *Monthly Notices of the Royal Astronomical Society* **517**, 4620–4636 (2022), ISSN 1365-2966, URL <http://dx.doi.org/10.1093/mnras/stac2744>.
- [47] M. Tristram, A. J. Banday, K. M. Górski, R. Keskitalo, C. R. Lawrence, K. J. Andersen, R. B. Barreiro, J. Borrill, H. K. Eriksen, R. Fernandez-Cobos, et al., *Astronomy & Astrophysics* **647**, A128 (2021), ISSN 1432-0746, URL <http://dx.doi.org/10.1051/0004-6361/202039585>.
- [48] M. Tristram, A. J. Banday, M. Douspis, X. Garrido, K. M. Górski, S. Henrot-Versillé, L. T. Hergt, S. Ilić, R. Keskitalo, G. Lagache, et al., *Astronomy & Astrophysics* **682**, A37 (2024), ISSN 1432-0746, URL <http://dx.doi.org/10.1051/0004-6361/202348015>.
- [49] G. Efstathiou and S. Gratton, *The Open Journal of Astrophysics* **4** (2021), ISSN 2565-6120, URL <http://dx.doi.org/10.21105/astro.1910.00483>.
- [50] M. S. Madhavacheril, F. J. Qu, B. D. Sherwin, N. MacCrann, Y. Li, I. Abril-Cabezas, P. A. R. Ade, S. Aiola, T. Alford, M. Amiri, et al., *The Astrophysical Journal* **962**, 113 (2024), ISSN 1538-4357, URL <http://dx.doi.org/10.3847/1538-4357/acff5f>.
- [51] F. J. Qu, B. D. Sherwin, M. S. Madhavacheril, D. Han, K. T. Crowley, I. Abril-Cabezas, P. A. R. Ade, S. Aiola, T. Alford, M. Amiri, et al., *The Astrophysical Journal* **962**, 112 (2024), ISSN 1538-4357, URL <http://dx.doi.org/10.3847/1538-4357/acfe06>.
- [52] J. Carron, M. Mirmelstein, and A. Lewis, *Journal of Cosmology and Astroparticle Physics* **2022**, 039 (2022), ISSN 1475-7516, URL <http://dx.doi.org/10.1088/1475-7516/2022/09/039>.
- [53] H. T. Jense, M. Viña, E. Calabrese, and J. C. Hill, *Physical Review D* **113** (2026), ISSN 2470-0029, URL <http://dx.doi.org/10.1103/ff9j-skyj>.
- [54] B. Popovic et al. (DES) (2025), 2511.07517.
- [55] K. Lodha et al. (DESI), *Phys. Rev. D* **112**, 083511 (2025), 2503.14743.
- [56] G. Gu et al. (DESI), *Nature Astron.* **9**, 1879 (2025), [Erratum: *Nature Astron.* 9, 1898 (2025)], 2504.06118.
- [57] A. R. Liddle, *Monthly Notices of the Royal Astronomical Society: Letters* **377**, L74–L78 (2007), ISSN 1745-3925, URL <http://dx.doi.org/10.1111/j.1745-3933.2007.00306.x>.

### Appendix A: Dovekie results

A recent reanalysis of the DES Supernova dataset, designed as DESY5-Dovekie [54], has been released. These updated data reduce the tension between  $\Lambda$ CDM and  $\omega_0\omega_a$ CDM from  $4.2\sigma$  to  $3.2\sigma$ , thereby mitigating the shift towards an evolving dark energy scenario. Given these findings, and considering the dataset tensions discussed in Section III B, it was necessary to investigate the  $\omega_0\omega_a$ CDM scenarios with negative neutrino masses using this new dataset to assess any emerging shifts. Figures 8 and 9 show the resulting posteriors, comparing the original DESY5 with DESY5-Dovekie.

The implementation of the DES-Dovekie reanalysis demonstrates that the posterior distribution for  $\sum m_{\nu,eff}$  remains essentially invariant, even when other parameters, like  $\Omega_m$ , exhibit noticeable shifts. The fact that the neutrino mass sum is preserved under this updated calibration reinforces the robustness of our main findings, confirming that our primary results are insensitive to this specific treatment.

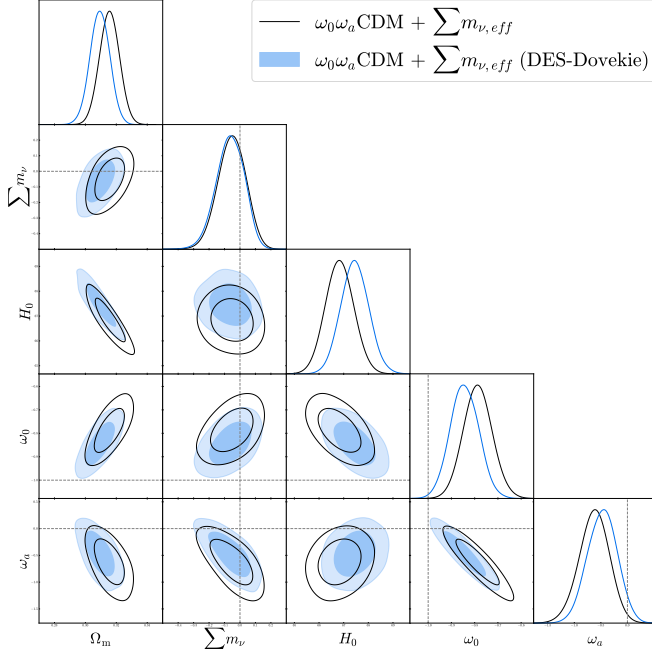


FIG. 8: Comparison of the  $\omega_0\omega_a$ CDM +  $\sum m_{\nu,eff}$  model between DESY5 and DESY5-Dovekie datasets. The reanalysis impacts several parameters, yet the neutrino mass posterior is invariant.

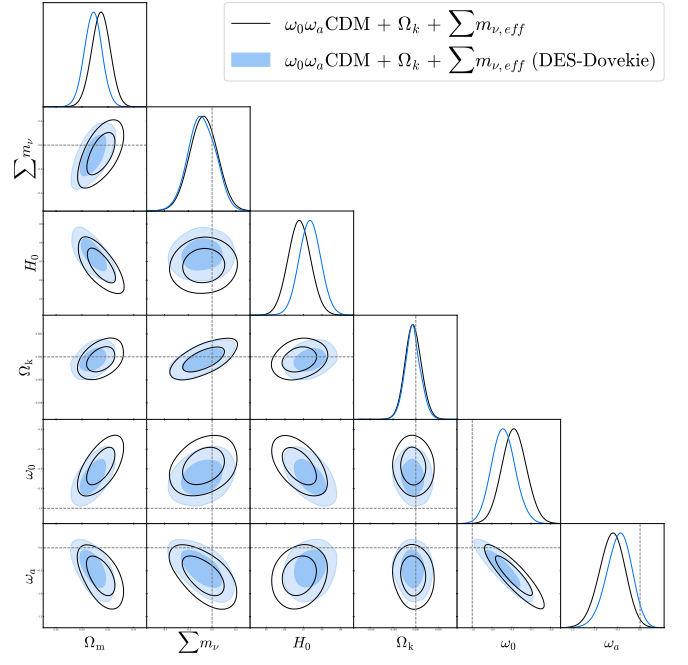


FIG. 9: Comparison of the  $\omega_0\omega_a$ CDM +  $\Omega_k$  +  $\sum m_{\nu,eff}$  model between DESY5 and DESY5-Dovekie datasets. As in Figure 8, the  $\sum m_{\nu,eff}$  distribution is unaffected by the reanalysis, and  $\Omega_k$  exhibits a similar behavior.

## Appendix B: Best-fit results for all cosmological parameters

To maintain clarity in the main discussion, the detailed results for the extended parameter set have been moved to this appendix.

Model	$\Omega_m$	$\Omega_{\text{edm}}h^2$	$\Omega_b h^2$	$H_0$ [km s $^{-1}$ Mpc $^{-1}$ ]	$100\theta_s$	$\ln(10^{-9}A_s)$	$n_s$	$\tau$	$10^9\Omega_k$	$\sum m_\nu$ [eV]	$\omega_0$	$\omega_n$
$\Lambda$ CDM	$0.3049 \pm 0.0036$	$0.11814 \pm 0.00061$	$0.02230 \pm 0.00012$	$68.03 \pm 0.27$	$1.04096 \pm 0.00023$	$3.051 \pm 0.013$	$0.9681 \pm 0.0033$	$0.0591^{+0.0066}_{-0.0073}$	-	-	-	-
$\Lambda$ CDM + $\sum m_\nu$	$0.3035 \pm 0.0036$	$0.11841 \pm 0.00064$	$0.02229 \pm 0.00012$	$68.17 \pm 0.29$	$1.04094 \pm 0.00023$	$3.047 \pm 0.013$	$0.9673 \pm 0.0034$	$0.0572 \pm 0.0070$	-	$< 0.0731$	-	-
$\Lambda$ CDM + $\Omega_k$	$0.3058 \pm 0.0036$	$0.1200 \pm 0.0011$	$0.02218 \pm 0.00014$	$68.35 \pm 0.32$	$1.04075 \pm 0.00026$	$3.048^{+0.011}_{-0.013}$	$0.9637 \pm 0.0039$	$0.0568^{+0.0064}_{-0.0073}$	$2.5^{+1.2}_{-1.4}$	-	-	-
$\Lambda$ CDM + $\Omega_k$ + $\sum m_\nu$	$0.3055^{+0.0039}_{-0.0044}$	$0.1200 \pm 0.0011$	$0.02218 \pm 0.00014$	$68.36 \pm 0.34$	$1.04074 \pm 0.00026$	$3.047 \pm 0.013$	$0.9636 \pm 0.0041$	$0.0556 \pm 0.0072$	$2.3^{+1.2}_{-1.4}$	$< 0.135$	-	-
$\omega_0\omega_n$ CDM + $\sum m_\nu$	$0.3187 \pm 0.0057$	$0.11919 \pm 0.00083$	$0.02224 \pm 0.00013$	$66.75 \pm 0.56$	$1.04082 \pm 0.00024$	$3.041 \pm 0.013$	$0.9654 \pm 0.0036$	$0.0539 \pm 0.0072$	-	$< 0.130$	$-0.758 \pm 0.059$	$-0.82^{+0.26}_{-0.21}$
$\omega_0\omega_n$ CDM + $\Omega_k$	$0.3187 \pm 0.0059$	$0.1196 \pm 0.0011$	$0.02222 \pm 0.00014$	$66.87 \pm 0.62$	$1.04079 \pm 0.00026$	$3.042 \pm 0.013$	$0.9645 \pm 0.0040$	$0.0537 \pm 0.0071$	$0.9^{+1.4}_{-1.6}$	-	$-0.774^{+0.073}_{-0.057}$	$-0.76^{+0.29}_{-0.25}$
$\omega_0\omega_n$ CDM + $\Omega_k$ + $\sum m_\nu$	$0.3190 \pm 0.0061$	$0.1196 \pm 0.0012$	$0.02222 \pm 0.00014$	$66.85 \pm 0.61$	$1.04078 \pm 0.00027$	$3.042 \pm 0.014$	$0.9647 \pm 0.0042$	$0.0538 \pm 0.0074$	$0.9^{+1.4}_{-1.6}$	$< 0.171$	$-0.773^{+0.074}_{-0.060}$	$-0.76^{+0.28}_{-0.30}$
$\Lambda$ CDM + $\sum m_{\nu,\text{eff}}$	$0.2992 \pm 0.0045$	$0.11928 \pm 0.00083$	$0.02221 \pm 0.00013$	$68.54 \pm 0.37$	$1.04177 \pm 0.00023$	$3.036 \pm 0.014$	$0.9645 \pm 0.0037$	$0.0521 \pm 0.0076$	-	$-0.073^{+0.051}_{-0.064}$	-	-
$\Lambda$ CDM + $\Omega_k$ + $\sum m_{\nu,\text{eff}}$	$0.3013 \pm 0.0054$	$0.1198 \pm 0.0011$	$0.02218 \pm 0.00014$	$68.55 \pm 0.39$	$1.04173 \pm 0.00024$	$3.038 \pm 0.015$	$0.9633 \pm 0.0040$	$0.0521 \pm 0.0077$	$1.1^{+1.5}_{-1.7}$	$-0.011^{+0.052}_{-0.050}$	-	-
$\omega_0\omega_n$ CDM + $\sum m_{\nu,\text{eff}}$	$0.3156 \pm 0.0063$	$0.11944 \pm 0.00087$	$0.02221^{+0.00013}_{-0.00014}$	$66.83 \pm 0.56$	$1.04175 \pm 0.00024$	$3.034 \pm 0.015$	$0.9640 \pm 0.0038$	$0.0509 \pm 0.0076$	-	$-0.052^{+0.095}_{-0.084}$	$-0.787 \pm 0.061$	$-0.63^{+0.29}_{-0.26}$
$\omega_0\omega_n$ CDM + $\Omega_k$ + $\sum m_{\nu,\text{eff}}$	$0.3146 \pm 0.0071$	$0.1191 \pm 0.0012$	$0.02225 \pm 0.00014$	$66.78 \pm 0.60$	$1.04177 \pm 0.00025$	$3.031 \pm 0.016$	$0.9652 \pm 0.0043$	$0.0503 \pm 0.0079$	$-0.6^{+1.6}_{-1.9}$	$-0.07 \pm 0.11$	$-0.786 \pm 0.061$	$-0.61^{+0.29}_{-0.26}$

TABLE V: Cosmological parameter constraints for all analyzed models. All values are reported at 68% confidence level, except for  $\sum m_\nu$ , which corresponds to the 95% upper limit.